
Flow, Turbulence and Combustion **71:** 105–118, 2003.

Separation and Turbulence Control in Biomimetic Flows

ALEXANDRA H. TECHET, FRANZ S. HOVER and
MICHAEL S. TRIANTAFYLLOU
Department of Ocean Engineering, Massachusetts Institute of Technology, Cambridge, MA 02139, U.S.A.; E-mail: mistetri@mit.edu

Received 2 October 2002; accepted in revised form 3 October 2003

Abstract. The study of the flow around live marine animals and robotic mechanisms which emulate fish motion has revealed a number of mechanisms of flow control, optimised through evolution to minimize the energy required for steady and unsteady motion underwater. We outline some of the mechanisms used to (a) eliminate separation, (b) reduce turbulence, and (c) extract energy from oncoming vortical flows.

Key words: biomimetic flows, separation control, turbulence control.

1. Introduction

Work with swimming fish and marine mammals has revealed a new paradigm of locomotion, distinctly different from conventional propulsion used in man-made vehicles [33, 34]. Fish employ relatively large amplitude, rhythmic unsteady body motions. These motions are used by swimming animals to achieve high efficiency and outstanding maneuvering agility [16]. Biomimetic studies and observations of fish and cetaceans have provided a wide array of information on the kinematics, i.e. how these animals employ their flapping tails and several fins to produce propulsive and maneuvering forces (see reviews in [13, 34]). Recent work with live animals provides important information on the resulting flow structures behind swimming fish [2, 8, 9, 19, 21, 23, 36]. Unsteady *fish-like* swimming motions have been studied experimentally in order to better understand how fish use their body motions to control separation, turbulence and vorticity; results from these experiments are discussed herein.

Unsteady motions have been used in laboratory and theoretical studies in the past to achieve flow control. Taneda [26] and Tokomaru and Dimotakis [31] imposed a rotational oscillation on a two-dimensional cylinder in cross-flow, reducing the width of the wake and hence the drag coefficient significantly, for properly selected parametric values. Injection of unsteady vorticity is the mechanism through which the flow control was implemented. Ffowcs-Williams and Zhao [12] also have shown that is possible to obtain efficient flow control through the unsteady

motion of a body in fluid. Maxworthy [20], Ellington [10, 11], Freymuth [14] and Dickinson [6, 7] studied the aerodynamics related to the flight of hovering insects and concluded that unsteady flow mechanisms play a very important role.

The possibility of extracting energy from oncoming vortices through an oscillating foil was investigated experimentally by Gopalkrishnan et al. [15]; and theoretically by Wu and Chwang [37], Sparenberg and Wiersma [22], and Streitlien and Triantafyllou [24, 25]. It was shown that energy contained in large-scale eddies can be retrieved hence enhancing propulsive efficiency, or amplifying thrust production.

We outline evidence of flow control achieved in fish-like swimming, including separation elimination and turbulence reduction, up to Reynolds numbers of 1.5×10^6; as well as energy extraction from oncoming vortical flows.

2. Separation and Turbulence Control

A flat plate undergoing transverse oscillations in the form of a traveling wave, placed in an oncoming steady flow, was found to exhibit reduced turbulence intensity and separation as the phase speed of the traveling wave is increased to reach values comparable to the free stream velocity [26]. The same mechanism of unsteady vorticity injection appears to control separation and turbulence production. The Reynolds number based on flat plate length was below 250,000, so it is important for applications to investigate much higher Reynolds numbers.

2.1. METHODOLOGY

Several mechanisms have been designed to study fish-like swimming motions. These mechanisms emulate the motion observed in live swimming fish, but do not attempt to model the feedback flow control that a live fish employs through the use of its lateral line sensing mechanisms. The first mechanism is the MIT RoboTuna, an eight link, tendon and pulley driven robot, whose external shape has the form of a Bluefin Tuna [32], capable of emulating the swimming motion of a live tuna. The second two mechanisms, a waving plate mechanism and a flapping foil device, aim to investigate respectively: traveling wave motion effects on near boundary flow and the energy extraction from oncoming vortical flows by flapping foil devices.

The RoboTuna is an eight link, pulley-driven robot modeled after the swimming motion and geometry of a Bluefin Tuna [32]. It is mounted on a carriage at the MIT Testing Tank, a towing tank 100 feet long, eight feet wide and five feet deep on average capable of towing speeds up to 1.5 m/s. Figure 1 shows the RoboTuna attached to the tank carriage (at left) with its lycra skin and the image at right shows the inside linkages that comprise part of the robot skeletal system.

Experimental work with a 1-meter flapping plate in a recirculating water tunnel at Reynolds numbers up to 2,000,000 shows reduction or even elimination of separation, and significant reduction of turbulence intensity as ration of the traveling

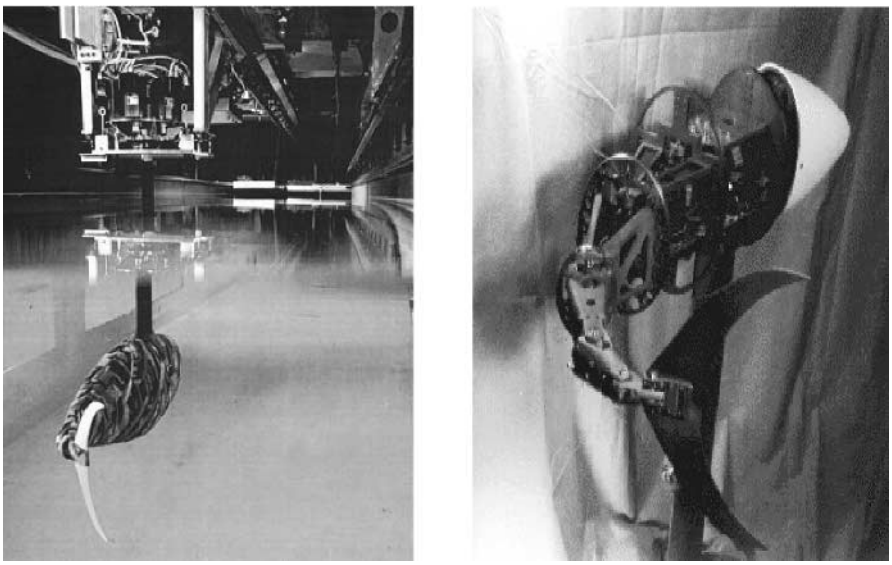

Figure 1. MIT RoboTuna. At left the robot swimming in the MIT Testing Tank attached to a towing carriage. At right, the inside structure of the RoboTuna allows the complex body motion of a swimming fish to be emulated. (Original in colour)

wave speed, c, to the freestream flow speed, U, approaches $c/U = 1.2$ [30]. Figure 2 shows a sketch of the experimental apparatus, which allows for a traveling wave motion using a series of scotch yokes driven by a single motor, activating eight pistons. The rods are connected to a reinforced rubber mat that forms the flapping plate.

The waving plate mechanism is designed using a flexible neoprene mat with eight pistons driving a traveling wave down the length of the mat. The apparatus was mounted in a recirculating water tunnel capable of speeds up to 9 m/s. The tunnel has a working section of 0.5 m by 0.5 m by 1.2 m long. The drive mechanism shown in Figure 2 atop the tunnel section is comprised of eight piston rods, which pass through a sealed window in the top of the tunnel section, controlled by a drive shaft coupled to the piston cranks arms by chain linkage. The mat is a structurally reinforced neoprene mat that is 1.4 m long and 0.5 m wide, spanning the tunnel. At the leading edge of the mat is an aluminum plate rigidly attached to the tunnel such that the amplitude at this point is zero. The motion has an amplitude envelope with slope 1/16, increasing to the stern. The mat length is 1.25 times the traveling wave wavelength. The phase speed, c, of the traveling wave is dictated by the speed of the drive shaft.

Data on the waving plate and RoboTuna mechanism were taken using a Digital Particle Image Velocimetry technique, where a laser sheet illuminates neutrally buoyant particles seeded throughout the fluid and a CCD camera records the motion of the particles in order to calculate the velocity vectors. An overview of this technique can be found in [1, 35]. In the case of the RoboTuna a Pulnix TM-1040

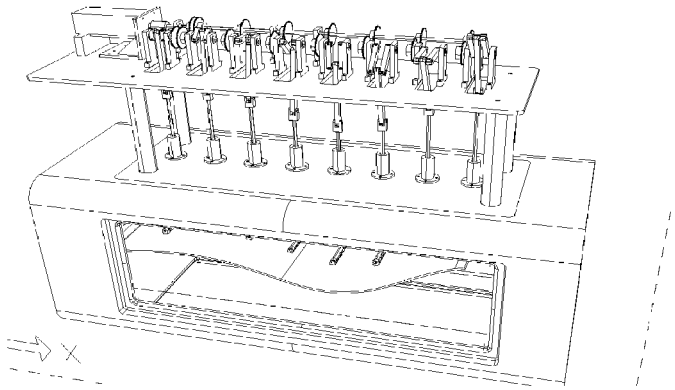

Figure 2. Sketch of the waving plate apparatus showing the drive mechanism and the piston configuration. The waving mat can be seen through the tunnel section side window. Flow is from left to right and the traveling wave propagates in the direction of the flow, with increasing amplitude, A ($A = x/16$, where $x = 0$ m is the leading edge of the mat). The drive mechanism is atop the tunnel and connected to the mat via eight piston rods.

camera, with 1024×1024 pixels and 30 Hz, was submerged in a watertight housing looking down on the robot with a light sheet, generated by a Spectra Physics PIV 400 mJ/pulse ND:Yag laser, entering the tank on a horizontal plane along the fish's lateral line (the mid-line between the dorsal (top) and anal (bottom) sides of the fish). For the waving plate the laser sheet, from a NewWave Gemini PIV 120 mJ/pulse ND:Yag laser, was oriented vertical coming in through the bottom window in the tunnel section and the Pulnix camera viewed the particle motions through the side window. In addition to PIV, a Dantec Laser Dopplar Velocimetry (LDV) was used to measure the boundary layer profile on the waving mat.

2.2. RESULTS

Flow visualization with the 1.20 m long robotic mechanism, the RoboTuna, exhibited lack of separation effects along its body, even when the motion amplitude reached values 10% of the body length. Also, measurement of the flow characteristics of the boundary layer, using particle image velocimetry (PIV) techniques, showed apparent re-laminarization of the flow when the traveling wave phase speed was close in value to the stream velocity [3, 27–29].

Under conditions of towing the mechanism without transverse motion, the boundary layer was characterized by a turbulent velocity profile. Figure 3 demonstrates the difference between the two measured average velocity profiles: The form of the velocity curve has the characteristic law of the wall shape when there is no transverse motion, while a laminarized shape appears when there is active swimming motion with $c/U = 1.14$, where c is the speed of the traveling wave along the body length and U the speed of the external stream. The solid line fits

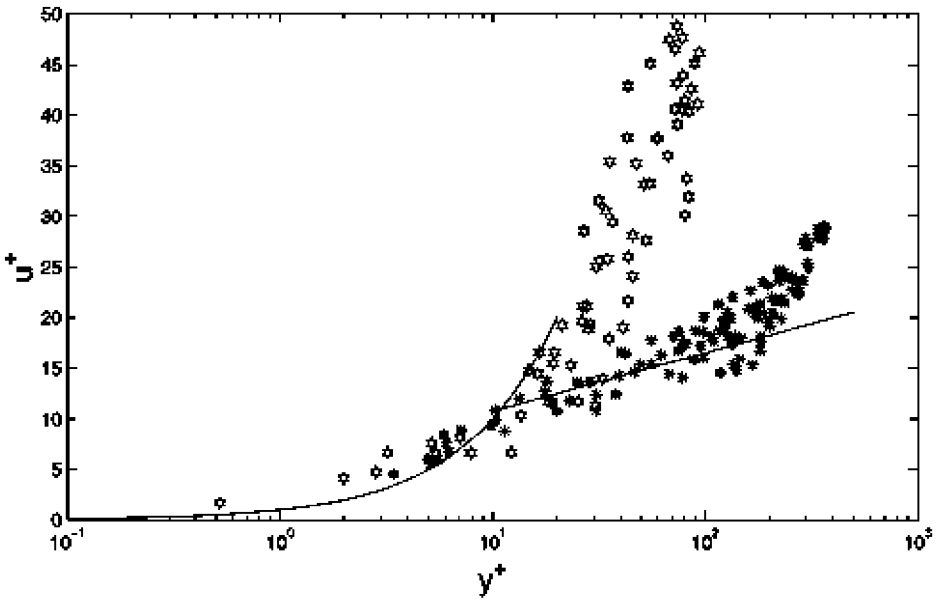

Figure 3. Comparison of the near boundary average streamwise velocity profiles obtained with digital particle image velocimetry (DPIV) about the MIT RoboTuna at Reynolds number 800,000, based on the fish body length. Red (solid) symbols represent the non-swimming profile and are indicative of a turbulent boundary flow. The blue symbols represent the swimming case at $c/U = 1.14$; this profile indicates a laminarization of the near body flow. The solid line fits the 'law-of-the-wall' profile to the boundary layer data for the non-swimming fish for a baseline comparison. (Original in colour)

the 'law-of-the-wall' profile to the boundary layer data for the non-swimming fish for a baseline comparison.

Computational studies on a flat plate undergoing traveling wave oscillations within an oncoming stream, show reduction of separation as the phase speed c increases, with complete elimination of separation at c/U close to 1 [38]. Similarly, turbulence intensity is found to decrease non-uniformly across the length of the plate, with increasing c/U, up to a value of about 1.5. The study was conducted at Reynolds number, based on plate length, of 6,000 and then 18,000.

Although the flow features around the plate change with Reynolds number for a non-vibrating plate, the flow remains qualitatively similar at the Reynolds numbers studied when c/U is near 1, with a preferred value of $c/U = 1.2$. The energy to propel the flapping plate, defined as the energy to tow the plate (which can be negative if the plate produces thrust) plus the energy to oscillate the plate, is minimal at a value of $c/U = 1.2$ [38, 39]. Figure 4 shows the turbulence intensity along the length of a flapping plate, for two values of c/U, 0.4 and 1.2. There is non-uniform, but substantial reduction of turbulence intensity in the case of $c/U = 1.2$.

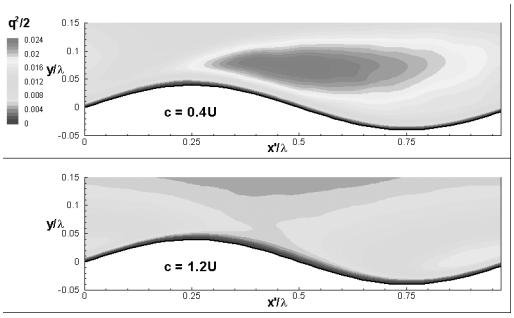

Figure 4. Direct Numerical Simulation (DNS) results show the turbulence intensity over a waving plate at Reynolds number 6,000. Plot at left is for phase speed, $c = 0.4U$ and at right is $c = 1.2U$. The red color indicates high levels of turbulence and the blue, low levels. As phase speed increases turbulence energy is progressively reduced, as indicated by the reduction of red color in the right image. (Original in colour)

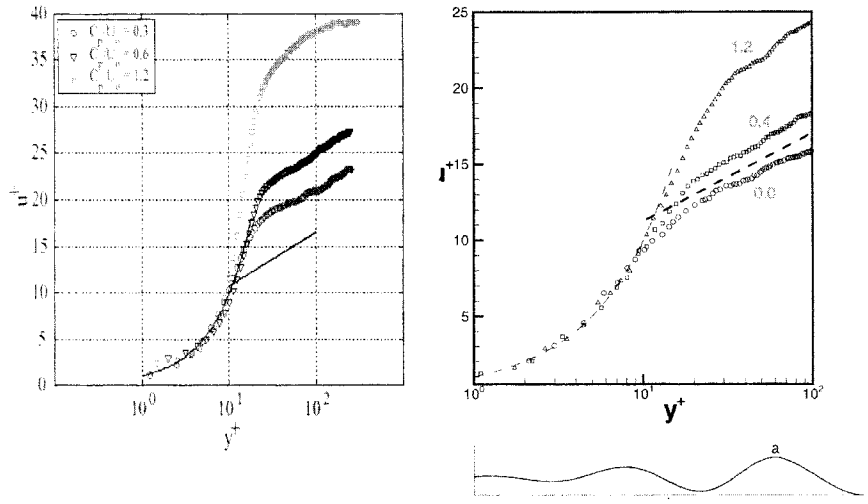

Figure 5. Comparison of PIV data from the waving plate experiment (left) at Reynolds numbers 10^6, based on mat length, and direct numerical simulations (DNS) (right) at Reynolds number 6,000. The figures show persistence of laminarization through traveling wave motion at higher Reynolds number than previously investigated. Data sets represent boundary layer profiles at a mat crest. Three wave phase speeds are represented by each of the data sets. For the experimental data the phase speed to freestream velocity rations are $c/U = 0.3$, 0.6 and 1.2 are shown in red, blue, and green respectively; for the DNS data the ratios shown are $c/U = 0.0$, 0.4, and 1.2, in circle, squares and triangles respectively. The solid line (left) and dashed line (right) is a fit to the 'law of the wall' turbulent boundary layer profile. (Original in colour)

Figure 5 shows a comparison between digital particle image velocimetry (DPIV) data at Reynolds numbers 10^6 and direct numerical simulations at Reynolds number 6,000, demonstrating the qualitative similarity between the two cases, despite the large difference in Reynolds number. Figure 6 shows the phase averaged turbulence intensity of the horizontal (streamwise) and vertical components of the velocity normalized with respect to U^2, the square of the average freestream flow speed. The turbulence intensity is calculated from ensemble averaged laser Doppler velocimetry (LDV) records. The total velocity is $U_t = u + U$, where u is the turbulence fluctuation and U is the average flow velocity obtained from phase averaged velocity samples (sample size $N = 1000$). The velocity measured 4mm under the mat boundary at piston #5 (fifth piston aft of leading edge). The inflow velocity is $U = 1.0$ m/s and the phase speed varies from $c/U = 0.3$ to 2.0. As shown, the local turbulence intensity is reduced for c/U up to 1.5, but increases for phase speeds beyond this value.

Recent studies with a three-dimensional body, in the form of a water snake, undergoing traveling wave oscillations, identical to those studied with the flapping plate mechanism, shows non-uniform turbulence reduction along the body, but the clear trends observed with a two-dimensional plate could not be established [17].

3. Energy Extraction from Oncoming Vortical Flows

Anecdotal evidence of energy recovery by live fish in turbulent flow containing large scale eddies is substantiated by experimental work with live fish [5]; and with simpler experiments using the controlled motion of a flapping foil within the wake of a bluff body, such as a D-section cylinder. The foil is used to extract energy from the flow by properly timing its motion relative to the arrival of large eddies [15, 4, 5].

Gopalkrishnan et al. [15] placed a two-dimensional foil in the wake of a cylinder within an oncoming stream to measure the forces and torque needed to oscillate the foil so as to produce thrust; and to observe the flow patterns around the oscillating foil. The foil would undergo a flapping motion, i.e. harmonic, controlled heave (transverse) and pitch (angular) motions with adjustable amplitude and relative phase. They found that depending on the timing of the motion of the foil relative to the arrival of oncoming vortices, three distinct patterns could be observed:

- A destructive interference pattern, where vortices shed by the foil would first pair and then coalesce with opposite-sign vortices shed by the upstream cylinder to form a wake consisting of weak vortices aligned near the centerline of the wake. The efficiency of thrust production was found to be increased compared to other conditions.
- A constructive interference pattern, where vortices shed by the foil would coalesce with same-signed cylinder vortices forming strong vortices arranged in a

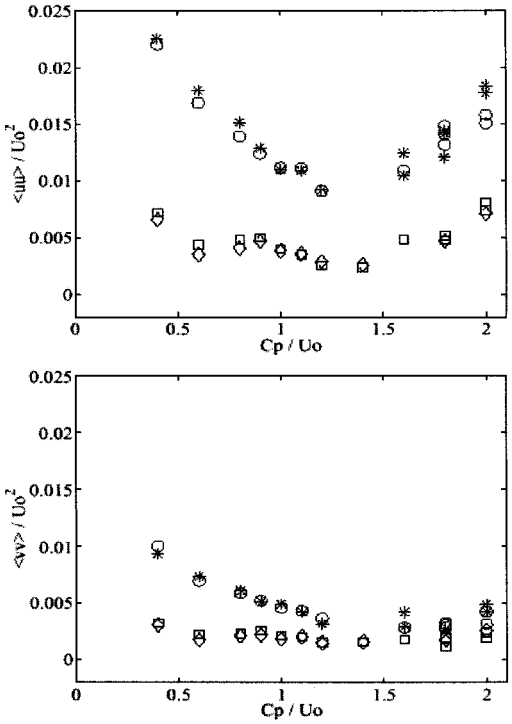

Figure 6. Normalized horizontal, $\langle uu \rangle / U^2$, and vertical, $\langle uu \rangle / U^2$, turbulent energy, respectively top and bottom, calculated from ensemble averaged LDV data recorded 4 mm under the mat boundary at piston #5. u is the fluctuation velocity and U is the mean flow speed. Inflow speed is $U = 1.0$ m/s and phase speed varies from $c/U = 0.3$–2.0. Local turbulence energetics are reduced for phase speed up to 1.5 times inflow speed, but increase for phase speeds beyond this value up to $c/U = 2.0$. Red data is taken in the mat trough and blue at the mat crest. (Original in colour)

von Kármán street or reverse von Kármán street, depending on the parametric conditions. Efficiency was found to be minimal under such conditions.

- An intermediate condition, where foil vortices would pair with opposite signed cylinder vortices forming 'mushroom'-like structures, expanding the wake width.

Theoretical studies by Streitlien & Triantafyllou [24, 25] showed that energy extraction is possible when a foil operates in the wake of a bluff body, in an 'intercepting' mode, where the foil would intercept with its leading edge oncoming vortices. Efficiency, defined as the ratio of the useful energy (thrust times free stream velocity) over expended energy, could exceed 100% under conditions of energy extraction. The flow patterns associated with the intercepting mode consist of opposite-signed vortices, one from the cylinder and the other from the foil, which are pushed close together, resulting in an effective mutual elimination (the inviscid

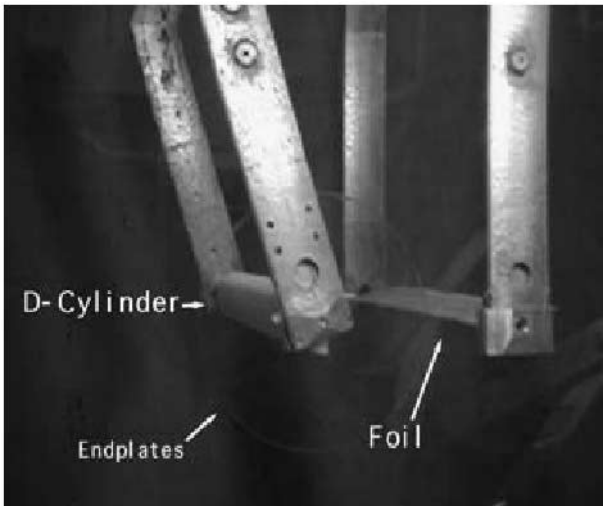

Figure 7. The foil-cylinder apparatus is shown above. The foil and cylinder are attached to an overhead carriage and move together down the tank. The D-cylinder moves sinusoidally in heave only, creating a von Kármán vortex street. The foil moves in heave and pitch and the phase of the motion follows the cylinder determining the interaction of the foil with the von Kármń wake. (Original in colour)

code could not predict destructive vortex interference, since two inviscid vortices of the opposite sign do not coalesce). A different mode, named 'slaloming mode', was characterized by the foil avoiding to intercept oncoming vortices (slaloming around them): Energy was not recovered and the resulting wake consisted of vigorous vortices resulting from coalescence of same signed vortices, one from the cylinder and the other from the foil.

3.1. METHODOLOGY

We employ a specially constructed apparatus (see Figure 7) at the MIT Testing Tank Facility, consisting of two inverted-U frames: The front frame supporting a bluff cylinder of diameter 7.5 cm, span 60 cm, and with a D-shaped cross-section (the flat portion facing downstream), capable of oscillating in an up and down motion; and the rear frame supporting a two dimensional NACA0012 foil, with chord 10 cm and span 60 cm, capable of executing a heave (up and down linear motion) and a pitch (angular motion about an axis located at about 1/3 of the chord from the leading edge). The cylinder and foil are towed at constant speed one behind the other, while executing independently-driven harmonic motions of given amplitude and phase. Circular end plates were fitted at both ends of the cylinder and foil to reduce end effects. The dimensions of the Tank are 30 m by 2.6 m by 1.14 m.

Pairs of lead-screws and linear tables were employed to achieve the linear motions of both the cylinder and the foil, powered by Parker ML3475B direct-drive

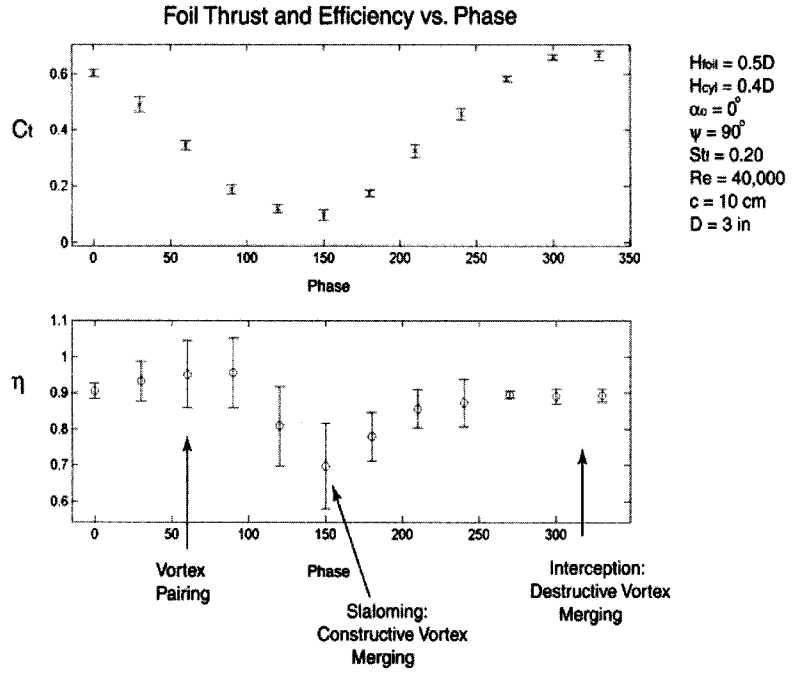

Figure 8. Foil thrust coefficient, C_t, and propulsive efficiency, ?? when placed behind a cylinder generating large scale eddies. The horizontal axis is the phase angle between foil motion and arrival of a cylinder vortex, which causes large changes in C_t and η due to vortex-foil interactions. The cylinder motion has a heave amplitude, $H_{\text{cyl}} = 0.4D$, where D is the cylinder diameter ($D = 7.5$ cm). The foil amplitude of motion is $H_{\text{foil}} = 0.5D$, amplitude of pitch angle is $\alpha_0 = 0°$, and heave-pitch phase angle is $\psi = 90°$. The Strouhal number is St $= 0.3$ and the Reynolds number $R_c = 40{,}000$, based on the foil chord length ($c = 10$ cm). (Original in colour)

motors and amplifiers; while the foil pitch motion was actuated through a chain and sprocket arrangement powered by a Pittman GM14900 geared servomotor. Forces were measured at the ends of the cylinder and foil through Kistler 9601 force cells and a 9069 torque cell. A potentiometer returned the pitch angle, and the linear motion was measured through an LVDT.

The foil was placed five cylinder diameters behind the cylinder, while the phase between the heave and pitch motion was fixed at 90°, while the heave amplitude of both the cylinder and foil was fixed at 7.5 cm. The frequency of motion was chosen to close to the Strouhal frequency of the cylinder, while the phase angle between the cylinder and foil motion, and the angle of attack of the foil were the major parameters of the testing program [5]. The phase angle between cylinder and foil motion controls the timing between the arrival of a von Kármán vortex generated by the cylinder and the position of the leading edge of the foil, which can, for example, intercept the vortex, or avoid it.

3.2. RESULTS

Figure 8 shows the thrust coefficient and efficiency of a flapping foil within the wake of a vortex-shedding cylinder. The thrust coefficient, C_t, is calculated from the measured thrust, T, as $C_t = 2T/(U^2cs)$, where U is the towing speed, c is the foil chord and s is the foil span. The foil efficiency is calculated as $\eta = TU/P_{\text{foil}}$, where P_{foil} is the power generated by the flapping foil. The foil power is calculated from the measured lift, L, and torque, τ, and heave, h, and pitch, θ, accelerations: $P_{\text{foil}} = L(\mathrm{d}h/\mathrm{d}t) + \tau(\mathrm{d}\theta/\mathrm{d}t)$.

As seen, both thrust coefficient and efficiency are affected significantly by the timing of vortex arrival. The relative timing between the arrival of cylinder-generated eddies and eddies shed by the trailing edge of the foil is crucial in determining the type of vortex interaction that will prevail. Visualization of the flow shows that the three principal patterns identified in [15] can be associated with the efficiency peaks (destructive interference mode), efficiency troughs (constructive interference mode), and efficiency nodes (vortex pairing). Efficiency can even exceed 100% due to energy recovery by the foil [4].

In the case of live fish, work with swimming trout in a water flume shows that when a bluff body is placed upstream of the animals, their regular swimming patterns change, and the frequency of body motion is synchronized with the frequency of vortex shedding from the cylinder. The body motion also changes, with the apparent trend that fish arrange for their body to intercept oncoming vortices, in agreement with the experimental findings from the airfoils [5]. Also, the wavelength of the body motion is changed to accommodate the frequency requirements of the upstream bluff body.

4. Conclusions

Experimental and numerical investigations of *fish-like* swimming motion explore the benefits of unsteady motion for the control of separation, turbulence, and vorticity. A traveling wave motion can reduce local turbulence levels significantly as shown through experiments and numerical simulations, especially in regions of high separation such as the wave trough; and experiments with an unsteady flapping foil in the wake of a heaving cylinder revealed energy extraction from an oncoming vortical wake.

To study separation elimination and turbulence reduction, first a robotic fish was constructed and tested, modeled after the bluefin tuna. The robot emulates the measured fish kinematics in water, which have the form of a structural wave traveling from the head to the tail. Flow visualization using DPIV near the fish's body, at an optimal wave speed of $c/U = 1.14$, reveals that the boundary layer of the actively swimming robot has an average velocity profile closely resembling a laminar boundary layer; whereas when towed rigid-straight the velocity profile has a turbulent boundary layer shape. Further investigation of the effect of traveling wave motion on the boundary layer of a flat plate was performed experimentally

and numerically. The two-dimensional plate undergoing traveling wave motion is a simpler structure than the three-dimensional surface of a *fish-like* body, which nonetheless captures the essence of the phenomena involved in turbulence reduction and separation elimination. It was shown that, over a wide range of Reynolds numbers, qualitatively similar mechanisms are at work, providing flow without separation, as well as spatially non-uniform reduction in turbulence intensity; these effects were found to be optimal when the phase speed is close to 1.2 times the free stream velocity.

To study energy extraction from oncoming turbulent flow, a special apparatus was used, consisting of an upstream bluff cylinder, which produces a regular von Kármán street when towed at constant speed; and a downstream foil, capable of executing a harmonic heaving and pitching motion. Under properly selected conditions, the foil can extract energy from the oncoming cylinder-generated eddies, hence augmenting its thrust and efficiency. Subsequent experiments with live fish and flexibly mounted foils, show that energy extraction is feasible both for flapping two-dimensional foils as well as swimming fish, and fish-like three-dimensional bodies. The flapping foil motion can be tuned to maximize propulsive efficiency, while live fish adapt to oncoming flow structures to minimize the required power to maintain position within an oncoming flow.

These experimental and numerical studies show that *fish-like* locomotion can employ mechanisms of flow control to achieve (a) separation elimination, (b) turbulence reduction and (c) energy extraction from oncoming flow, in order to minimize the energy needed for locomotion.

Acknowledgements

Support by ONR under contract N00014-00-1-0198 and by the MIT Sea Grant Program under Grant NA46RG0434 is gratefully acknowledged.

References

1. Adrian, R.J., Particle imaging techniques for experimental fluid mechanics. *Annual Rev. Fluid Mech.* **23** (1991) 261–304.
2. Anderson, J.M., Vortex control for efficient propulsion. Ph.D. Thesis, Joint Program, Massachusetts Institute of Technology & Woods Hole Oceanographic Institution (1996).
3. Anderson, E.J., McGillis, W.R., Grosenbaugh, M.A., Techet, A.H. and Triantafyllou, M.S., Visualization and analysis of boundary layer flow in swimming fish. In: *Proceedings of the First International Symposium on Turbulence & Shear Flow Phenomena*, Santa Barbara, CA (1999).
4. Beal, D.N., Hover, F.S. and Triantafyllou, M.S., The effect of a vortex wake on the thrust and efficiency of an oscillating foil. In: *Proceedings of the 12th International Symposium on Unmanned Untethered Submersible Technology (UUST01)*, Durham, NH (2001).
5. Beal, D.N., Propulsion through wake synchronization using a flapping foil. Ph.D. Thesis, MIT, Cambridge, MA (2003).

6. Dickinson, M.H., The effect of wing rotation on unsteady aerodynamic performance at low Reynolds numbers. *J. Exp. Biol.* **192** (1994) 179–206.
7. Dickinson, M.H., Lehmann, F.O. and Sane, S.P., Wing rotation and the aerodynamic basis of insect flight. *Science* **284** (1999) 1954–1960.
8. Drucker, E.G. and Lauder, G.V., Locomotor forces on a swimming fish: Three dimensional vortex wake dynamics quantified using DPIV. *J. Exp. Biol.* **202** (1999) 2393–2412.
9. Drucker, E.G. and Lauder, G.V., A hydrodynamic analysis of fish swimming speed: Wake structure and locomotor force in slow and fast labriform swimmers. *J. Exp. Biol.* **203** (2000) 2379–2393.
10. Ellington, C.P., The aerodynamics of hovering insect flight. *Philos. Trans. Roy. Soc. London, Ser. B* **305** (1984) 17–181.
11. Ellington, C.P., The novel aerodynamics of insect flight: Applications to micro-air vehicles. *J. Exp. Biol.* **202** (1999) 3439–3448.
12. Ffowcs-Williams, J. and Zhao, B., The active control of vortex shedding. *J. Fluids Struct.* **3** (1989) 115–122.
13. Fish, F.E. and Hui, C.A., Dolphin swimming – A review. *Mammal Rev.* **21**, 181–195.
14. Freymuth P., Thrust generation by an airfoil in hover modes. *Exps. Fluids* **9** (1990) 17–24.
15. Gopalkrishnan, R., Triantafyllou, M.S., Triantafyllou, G.S. and Barett, D.S., Active vorticity control in a shear flow using a flapping foil. *J. Fluid Mech.* **274** (1994) 1–21.
16. Harper, D.G. and Blake, R.W., Prey capture and the fast-start performance of northern pike (Essox Lucius). *J. Exp. Biol.* **155** (1991) 175–192.
17. Michel, A.P.M., Techet, A.H., Hover, F.S. and Triantafyllou, M.S., Experiments with an undulating snake robot. In: *Proceedings Oceans 2001*, Honolulu, HI (2001).
18. Kumph, J.M., Techet, A.H., Yue, D.K.P. and Triantafyllou, M.S., Flow control of flexible hull vehicles. In: *Proceedings of the 11th International Symposium on Unmanned Untethered Submersible Technology (UUST99)*, Durham, NH, August 22–25 (1999).
19. Lauder, G.V., 2000, Function of the caudal fin during locomotion in fishes: Kinematics, flow visualization and evolutionary patterns. *Amer. Zool.* **40** (2000) 101–122.
20. Maxworthy, T., Experiments on the Weis-Fogh mechanism of lift generation by insects in hovering flight. Part I. Dynamics of the fling. *J. Fluid Mech.* **93** (1979) 47–63.
21. Mueller, U., van den Heuvel, B., Stamhuis, E. and Videler, J., Fish foot prints: Morphology and energetics of the wake behind a continuously swimming mullet (*Chelon Labrosus Risso*). *J. Exp. Biol.* **200** (1997) 2893–2806.
22. Sparenberg, J.A. and Wiersma, A.K., On the efficiency increasing interaction of thrust producing lifting surfaces. In: Wu, T., Brokaw, C.W. and Brennen, C. (eds.), *Swimming and Flying in Nature*, Vol. 2 (1975) pp. 891–917.
23. Stamhuis, E. and Videler, J., Quantitative flow analysis around aquatic animals using laser sheet particle image velocimetry. *J. Exp. Biol.* **198** (1995) 283–294.
24. Streitlien, K. and Triantafyllou, M.S., Force and moment on a Joukowski profile in the presence of point vortices. *AIAA J.* **33** (1995) 603–610.
25. Streitlien, K., Triantafyllou, G.S. and Triantafyllou, M.S., Efficient foil propulsion through vortex control. *AIAA J.* **34** (1996) 2315–2319.
26. Taneda, S., Visual study of unsteady separated flows around bodies. *Progr. Aerosp. Sci.* **17** (1977) 287–348.
27. Techet, A.H. and Triantafyllou, M.S., Experimental study of a waving plate. In: *52nd Annual Meeting of the Division of Fluid Dynamics, American Physical Society*, New Orleans, LA, 21–24 November (1999).
28. Techet, A.H. and Triantafyllou, M.S., Near boundary visualization of the flow about fish-like swimming bodies. In: *53rd Annual Meeting of the Division of Fluid Dynamics, American Physical Society*, Washington, DC, November 19–21 (2000).

29. Techet, A.H., Triantafyllou, M.S., Anderson, E.J., McGillis, W.R. and Grosenbaugh, M.A., Boundary layer relaminarization in swimming fish. In: *Proceedings of the Symposium on Intern. Soc. Offshore & Polar Engineers (ISOPE'99)*, Brest, France, June (1999).
30. Techet, A.H., Experimental visualization of the near-boundary flow about fish-like swimming bodies. Ph.D. Thesis, MIT/WHOI, Cambridge/Woods Hole, MA (2001).
31. Tokomaru and Dimotakis, P., Rotary oscillation control of a cylinder wake. *J. Fluid Mech.* **224** (1991) 77–90.
32. Triantafyllou, M.S. and Triantafyllou, G.S., An efficient swimming machine. *Sci. Amer.* **272**(3) (1995) 64–70.
33. Triantafyllou, M.S., Yue, D.K.P. and Triantafyllou, G.S., Hydrodynamics of fish swimming. *Annual Rev. Fluid Mech.* **32** (2000) 33–53.
34. Videler, *Fish Swimming*. Chapman & Hall, London (1993).
35. Willert, C.E. and Gharib, M., Digital particle image velocimetry. *Exp. Fluids* **10** (1991) 181–193.
36. Wolfgang, M.J., Anderson, J.M., Grosenbaugh, M.A., Yue, D.K.P. and Triantafyllou, M.S., Near-body flow dynamics in swimming fish. *J. Exp. Biol.* **202** (1999) 2303–2327.
37. Wu and Chwang, Extraction of flow energy by fish and birds in a wavy. In: Wu, T., Brokaw, C.J. and Brennen, C. (eds.), *Swimming and Flying in Nature*, Vol. 2 (1975) pp. 687–702.
38. Zhang, X., Direct numerical simulation of the flow over a flexible plate. Ph.D. Thesis, MIT, Cambridge, MA (2001).
39. Shen, L., Zhang, X., Triantafyllou, M.S. and Yue, D.K.P., Turbulent flow over a flexible wall undergoing a streamwise traveling wave motion. *J. Fluid Mech.* **484** (2003) 197–221.